INVITED ARTICLE

TECHNOLOGY

Physics-based computer simulation of the long-term effects of cardiac regenerative therapies

Lik Chuan Lee[1], Joakim Sundnes[2], Martin Genet[3] & Samuel T. Wall[2]

In this paper, we describe the application of an integrated electromechanics-growth computational model to simulate the long term effects of cardiac regenerative therapies in a left ventricle (LV). The electromechanics-growth model couples biophysically detailed cellular-based laws that describe the short term events occurring in the excitation-contraction coupling process in the cardiomyocytes, to a phenomenological law that describes the long-term process of growth and remodeling in the cardiac tissue. Two clinically relevant phases depicting the progression and subsequent treatment of heart failure were simulated using this model. These phases are namely, (1) the long-term remodeling process induced by a myocardial infarction and (2) the long-term response following regeneration of the infarct. Our model predictions show that the abnormal myofiber strain values surrounding the infarct can drive the post-infarct LV hypertrophy, whereas a subsequent normalization of the myofiber strain after infarct regeneration can lead to a reduction in the LV size. These findings are consistent with some of the observations found in the experiments and clinical studies of cardiac regenerative therapies.

***Keywords*: Myocardial Infarction; Growth and Remodeling; Finite Element Method; Cardiac Regenerative Therapy.**

INNOVATION

Computer modeling of heart disease treatments have mostly been confined to simulating their short-term effects. The novelty of this work lies in the application of a newly developed integrated electromechanics-growth computational model to simulate the long-term effects of cardiac regenerative therapies. This work is, to the best of our knowledge, the first simulation that directly models both the immediate and long-term mechanical effects when a non-contracting infarct is revived.

INTRODUCTION

Heart failure (HF) continues to pose a significant burden on our society. Between 2010 and 2030, the real cost of HF is projected to increase by a staggering 200%[1]. Among all HF conditions, 70% of them are of systolic origin with coronary artery diseases accounting for approximately two-thirds of these cases[2]. In the event of myocardial infarction (MI) in adult mammals, cardiomyocytes, unlike other cells, do not regenerate sufficiently to replace the lost ones. The end result of this is a permanent loss of contractile function in the infarcted region.

Current standard therapy for treating MI includes pharmacological treatments such as the admininstration of thrombolytic agents to restore coronary blood flow, and angiotensin-converting enzyme inhibitors to reduce blood pressure[3]. The long-term prognosis of MI remains poor. Although current treatments have improved MI survival significantly, around 24% of MI survivors still progress on to develop HF which has limited treatment options[4]. To address this issue, a myriad of new devices and treatments for MI have been developed in recent years, e.g. surgical ventricular restoration[5], ventricular partitioning device[6] and cardiac regenerative therapies[7,8].

Among these treatments, cell-based cardiac regenerative therapies have recently garnered a considerable interest. Multiple strategies are currently under investigation to regenerate diseased hearts. These strategies include the direct transplantation of stem cells into the infarcted myocardium, and the reprogramming of residing non-myocytes to cardiomyocytes in the diseased heart[7]. A number of clinical and experimental studies on these regenerative therapies have shown favorable post-treatment outcome in the form of an attenuation or a reversal of the adverse cardiac remodeling process[9,10]. The same positive outcome is, however, not found in other studies[11]. A better understanding on the mechanisms of cardiac regenerative therapies is, therefore, very much needed before they can be optimally applied to treat MI.

Computational models have been developed over the years to study a number of heart disease treatments[12–19]. While these models have been limited to simulating the immediate effects of the heart that results from a treatment, recent advancements in theory and model development have led to an emerging class of models that can describe the long term cardiac remodeling process[20–24]. A small number of these models have recently been used to evaluate the long-term effects of HF and treatments[24,25].

Here, we applied a recently developed electromechanics-growth model[26] to simulate the long-term effects of cardiac regenerative therapies. This growth model was established based on the principle that cardiomyocytes undergo hypertrophy or atrophy in order to restore strain

[1]Department of Mechanical Engineering, Michigan State University, East Lansing, MI 48824, USA, [2]Simula Research Laboratory, 1364 Fornebu, Norway, [3]Institute of Biomedical Engineering, ETH Zürich, 8092 Zurich, Switzerland. Correspondence should be addressed to: L.C.L. (lclee@egr.msu.edu).

Received 9 July 2015; accepted 13 January 2016; published online 4 March 2016; doi:10.1142/S2339547816400069

homeostasis[23]. Simulations using this model have shown that the collective long-term behavior of cardiomyocytes in response to an elevated and a reduced global mechanical loading results in, respectively, the dilation and shrinkage of the left ventricle (LV). This feature has been observed in hearts implanted with a left ventricular assist device[27]. Although the growth model has been used to simulate the long-term behavior of an LV with a non-contractile infarct[26], this model, however, has not been applied to simulate the case when the non-contractile infarct is regenerated and populated with contracting cardiomyocytes. By applying this model to simulate the first order effects of cardiac regenerative therapies here, we seek to test whether our model prediction is consistent with observations in experiments and clinical studies. Doing so will also enable us to understand how the surviving cardiomyocytes in the non-infarcted region will respond collectively to a regional restoration of the infarct contractile function.

METHODS

Electromechanics-growth model

Figure 1 shows a schematic of the electromechanics-growth model containing its key equations. The details of the model are given in Lee *et al.*[26] Here, we summarize the model with references to the equations given in the figure. Briefly, the model is an integration of a cardiac growth constitutive model[23] with a cardiac electromechanics model[28]. Cardiac electrophysiology was described by the bidomain equations (Equations 1,2), where $\mathbf{M}_i$, $\mathbf{M}_e$, v and v_e are, respectively, the intracellular, extracellular conductivity tensors (both scaled with the membrane capacitance and the cell membrane area to volume ratio), the transmembrane potential and the extracellular potential. A cellular electrophysiology model[29] was used to describe the exchange of ions across the cardiac cell membrane. This model was coupled to a cellular model describing the cross-bridge kinetics[30] via a vector of state variables $\mathbf{s}$, consisting of various membrane channels and intracellular ionic concentrations (Equation 3).

An active stress formulation was used to describe the mechanics of the cardiac tissue. In this formulation, the Cauchy stress tensor $\boldsymbol{\sigma}$ was additively decomposed into an active component $\boldsymbol{\sigma}_a$ and a passive component $\boldsymbol{\sigma}_p$. The active stress $\boldsymbol{\sigma}_a$ was described by a cellular-based cross-bridge model[30] (Equation 5) that was scaled by a parameter T that reflects the local tissue contractility. On the other hand, the passive stress $\boldsymbol{\sigma}_p$ was described by a prescribed Fung-type strain energy function W[31] (Equation 6). Near incompressibility of the tissue was enforced by splitting the strain energy function into a deviatoric component and a dilational component, and prescribing a large bulk modulus in the latter[32]. The stress tensor $\boldsymbol{\sigma}$ has to satisfy the balance of linear momentum equation (Equation 4).

Equations (1) to (6) describe the short term electromechanical behavior of the heart during a cardiac cycle. The cardiac cycle was simulated by first incrementally applying pressure to the LV endocardial surface until a prescribed end-diastolic pressure is reached. Systole was simulated by stimulating the LV apex. We note that this is a simplification of normal activation in the LV, which in actuality occurs through the Purkinje fiber system.

The LV cavity volume was constrained to remain constant during the isovolumic contraction phase until the LV pressure reached the prescribed aortic valve opening pressure. Thereafter, the ejection phase was simulated by coupling the LV cavity volume to a three-parameter Windkessel model (**Fig. 1**). Ejection ceased in the simulation when the LV volumetric flow rate becomes negative, and the LV cavity volume was constrained to remain constant during the subsequent isovolumic relaxation phase. Ventricular filling begin when the LV cavity pressure fell below a prescribed pressure and the cardiac cycle repeats itself.

To describe long-term cardiac growth, we used the theoretical volumetric-growth framework[33] in which the deformation gradient tensor $\boldsymbol{F}$ was multiplicatively decomposed into a growth tensor $\boldsymbol{F}_g$ and an elastic deformation tensor $\boldsymbol{F}_e$ (Equation 7). The growth tensor $\boldsymbol{F}_g$ was parameterized by a growth multiplier θ so that growth and reverse growth occur only along the cardiomyocyte long axis (Equation 8). A constitutive relationship was prescribed for θ so that growth or reverse growth occur only if the myocyte stretch is greater or lesser than a prescribed homeostatic stretch values (Equation 9), respectively. This constitutive

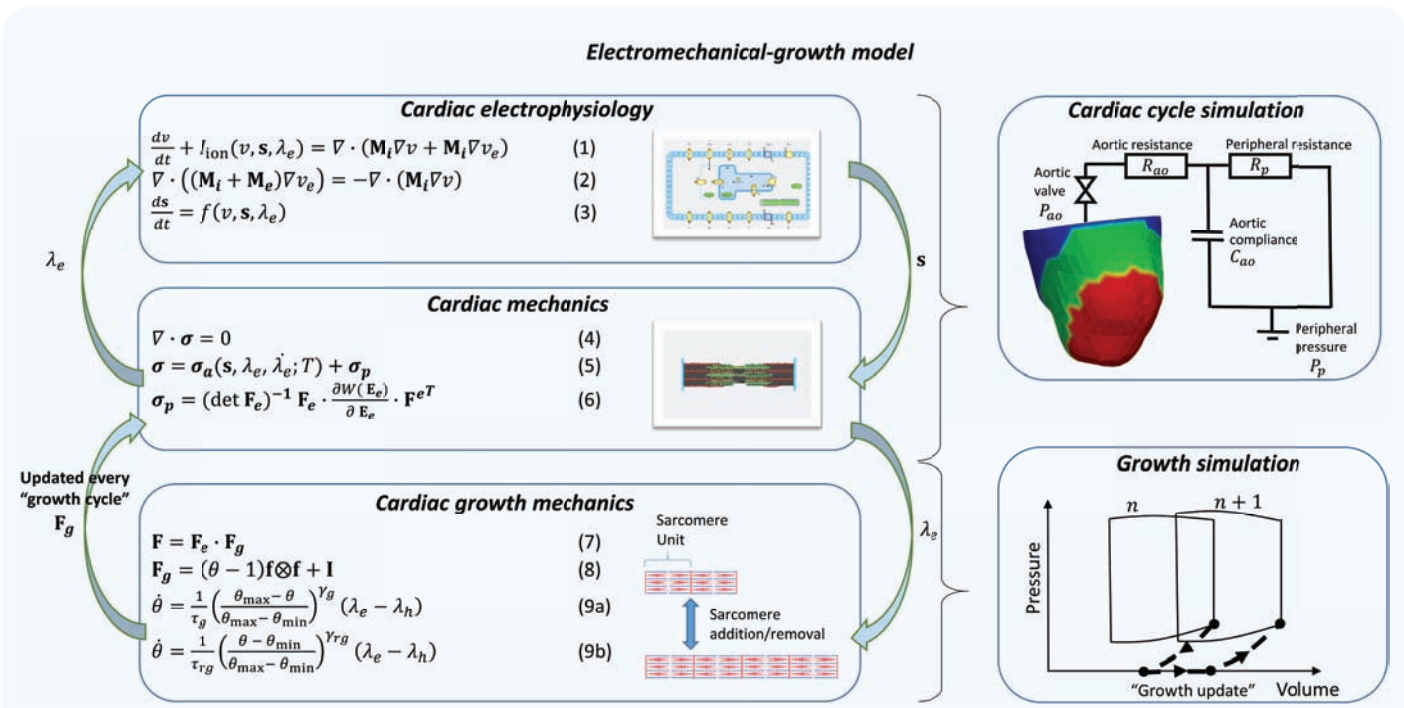

Figure 1 Schematic of the electromechanics-growth model.

relation was formulated based on previous experimental studies showing that (1) volume overload in ischemic cardiomyopathy causes cardiomyocytes to become elongated[34], and (2) this behavior can be reversed upon removal of the overloading conditions[35,36].

Because the cardiac growth model[23] and the electromechanics model[28] operate at two different timescales (i.e. growth and remodeling becomes appreciable only after a large number of heart beats), a separation of timescale was invoked to integrate the two models. Two assumptions are essential for separating the timescales. The first assumption is that growth and remodeling occurs too slowly to be detectable on the timescale of a single heartbeat. Correspondingly, the growth tensor $\boldsymbol{F}_g$ was assumed to be a constant within a cardiac cycle in our simulation. The second assumption is that the stimuli that drive growth and remodeling can be derived from a representative cardiac cycle. The simulation of a cardiac cycle then becomes equivalent to that of a "growth cycle" within which growth and remodeling is not detectable, and does not affect the electromechanics of the heart. By invoking these assumptions, the growth tensor was updated once every cardiac cycle at the end-of-diastole (**Fig. 1**). Specifically, the LV was unloaded at the end-of-diastole in each cycle and the updated growth tensor was then used to compute for the new "grown" unloaded geometry. Thereafter, the LV was loaded with the (same) prescribed end-diastolic pressure, and simulation of the cardiac cycle was resumed in the electromechanics model. This allows us to prescribe the time-averaged stretch over a cardiac cycle (or any other time-averaged quantities) as the growth stimulant for the cardiomyocytes[37].

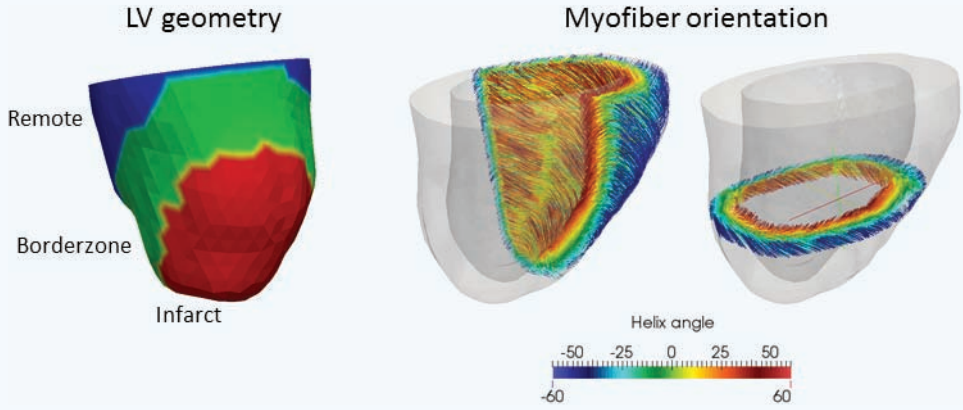

Figure 2 Schematic of the left ventricular (LV) infarct model and myofiber orientation color-coded with the prescribed myofiber helix angle.

Left ventricular geometry

The electromechanics-growth model was applied to a human LV geometry that was reconstructed from magnetic resonance images[38]. Three distinct regions were prescribed in the LV, namely, the infarct, borderzone and remote (healthy) regions. These regions differed from each other only in terms of the prescribed tissue contractility, a material parameter T (see Equation (5) in **Fig. 1** that is denoted by the "reference tension" in the active contraction model[30]). The infarct was assumed to be devoid of cardiomyocytes and, hence, was prescribed to be non-contractile and non-growing (i.e. $T_{\text{infarct}} = 0$). Because cardiomyocytes taken from the borderzone were found in experiments (using direct active force measurements) to have reduced contractility when compared to those taken from the remote region[39], the borderzone region was prescribed to have one-half the remote region's contractility in the simulation (i.e. $T_{\text{borderzone}} = 0.5\ T_{\text{normal}}$). Based on previous histological studies[40], the helix angle that defines the cardiomyocytes long axis was prescribed to vary linearly across the myocardial wall from −60° (endocardium) to 60° (epicardium) in the entire LV (**Fig. 2**). Local homeostatic time-averaged stretch values $\bar{\lambda}_e$ of the cardiomyocytes were obtained in another simulation using the same LV geometry in which both the infarct and borderzone have contractilities equal to that in the remote region (i.e. the same LV but with homogeneous normal contractility T_{normal}). Standard finite element method was used to solve the LV model comprising of 4,425 linear tetrahedral elements (maximum element size = 0.3 cm). Because the focus here is on cardiac mechanics, the same mesh was used to discretize the electrophysiology bidomain equations (Equations 1,2 in **Fig. 1**) and the mechanical equlibrium equation (Equation 4 in **Fig. 1**). We note that a finer mesh is required to yield accurate electrical wave propagation from the electrophysiology bidomain equations[41]. However, the current mesh is sufficient to obtain numerical convergence for the mechanical equilibrium equation. In addition to this, we also did not observe any locking phenomena which tetrahedral elements are prone to when the material is nearly incompressible with a large bulk modulus. Timesteps ranging between 1 and 50 milliseconds were employed in the simulation, with the systolic phase simulated using a smaller timestep and the diastolic phase simulated using a larger timestep. Details and parameter values of the model can be found in Lee *et al.*[26]

Simulation protocol

To simulate the effects of introducing new contractile cardiomyocytes into the infarct in cardiac regenerative therapies, the following two-phase simulation protocol was implemented. In the first phase — the remodeling phase, the LV model was ran for 5 growth cycles with impaired contractility in the infarct and the borderzone (i.e. $T_{\text{infarct}} = 0$; $T_{\text{borderzone}} = 0.5\ T_{\text{normal}}$). The healthy remote region was prescribed with a normal contractility (i.e. $T_{\text{remote}} = T_{\text{normal}}$). Then, in the second phase — the post-treatment phase, the infarct and borderzone contractilities were restored back to the normal values (i.e. $T_{\text{infarct}} = T_{\text{borderzone}} = T_{\text{normal}}$) and the LV model was ran for another 10 growth cycles. The value of T_{normal} was set to 60 kPa in the simulation. As a first approximation, we prohibited the infarct from growing in the entire simulation, and so we did not account for any possible growth in the infarct caused by the newly introduced cardiomyocytes. Our simulation therefore only considers the effects of the new cardiomyocytes in restoring the infarct contractility, and how that in turn affects the residing cardiomyocytes.

RESULTS

Pressure–volume relationship

Our simulation results showed a right shift of the pressure–volume (PV) loop during the remodeling phase (first five cycles) when a non-contractile infarct and a borderzone with depressed contractility were present in the LV. Compared to the LV with normal contractile function that had an ejection fraction (EF) of 49%[a], the infarcted LV showed a substantially smaller PV loop in the first cycle (EF = 32%) that shifted continuously towards the right in the next four cycles (EF at cycle 5 = 26%).

Restoration of the infarct and borderzone contractilities back to their normal values in the first cycle of the post-treatment phase led to an

[a] *Note*: the EF of 49% is slightly lower than the normal range of 55–70% that is typically found in normal humans.

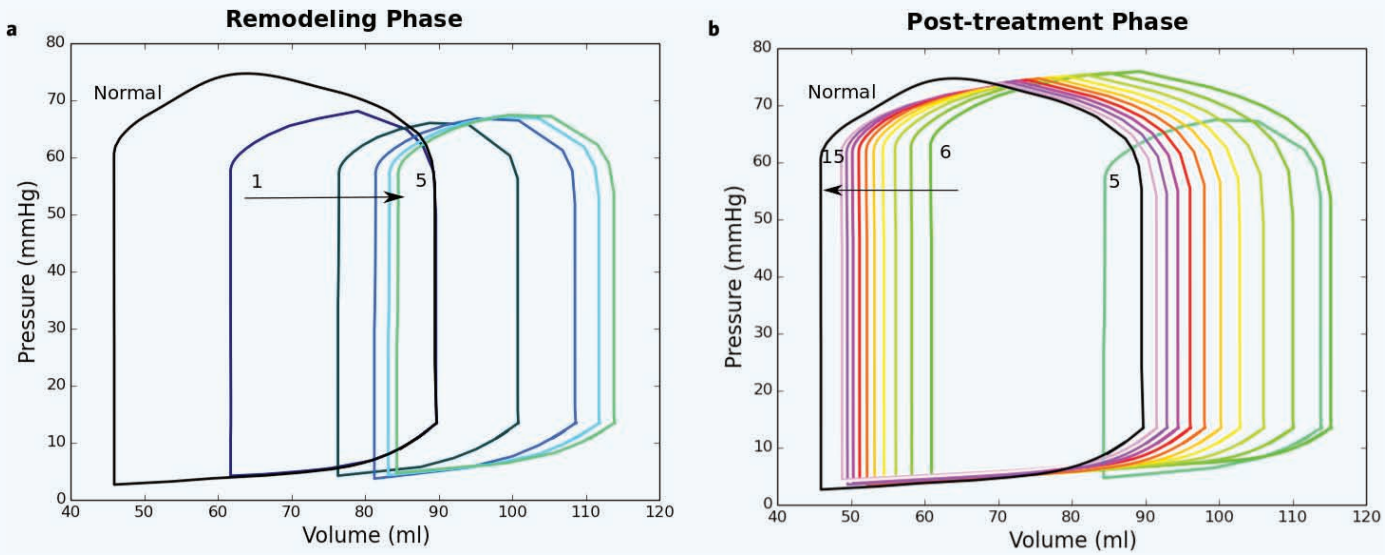

Figure 3 Pressure–volume (PV) loop during the (**a**) remodeling phase and (**b**) post-treatment phase.

expected larger PV loop (EF = 47%). In subsequent cycles, the PV loop shifted toward the left (**Fig. 3b**) and the EF was maintained.

Geometrical changes

The shifting of PV loops was reflected by a change in the LV geometry. During the remodeling phase, the LV became more dilated and spherical (**Fig. 4a**). Growth in the LV occurred primarily in the borderzone as indicated by the larger values of the determinant of the growth tensor det $\boldsymbol{F}_g$ found in that region. The larger values of det $\boldsymbol{F}_g$ reflects a lengthening of cardiomyocytes in the infarct borderzone.

During the post-treatment phase, the growth process was reversed and the LV became progressively smaller and more ellipsoidal (**Fig. 4b**). The growth tensor's determinant det $\boldsymbol{F}_g$ also decreased in the borderzone, reflecting a shortening of cardiomyocytes in its longitudinal axis.

Myofiber stretch

At the first cycle of the remodeling phase (cycle 1), the time-averaged elastic myofiber stretch $\bar{\lambda}_e$ was higher in both the infarct and borderzone when compared to that found in the same region in the normal LV (**Fig. 5**). In subsequent cycles during this phase, however, the borderzone

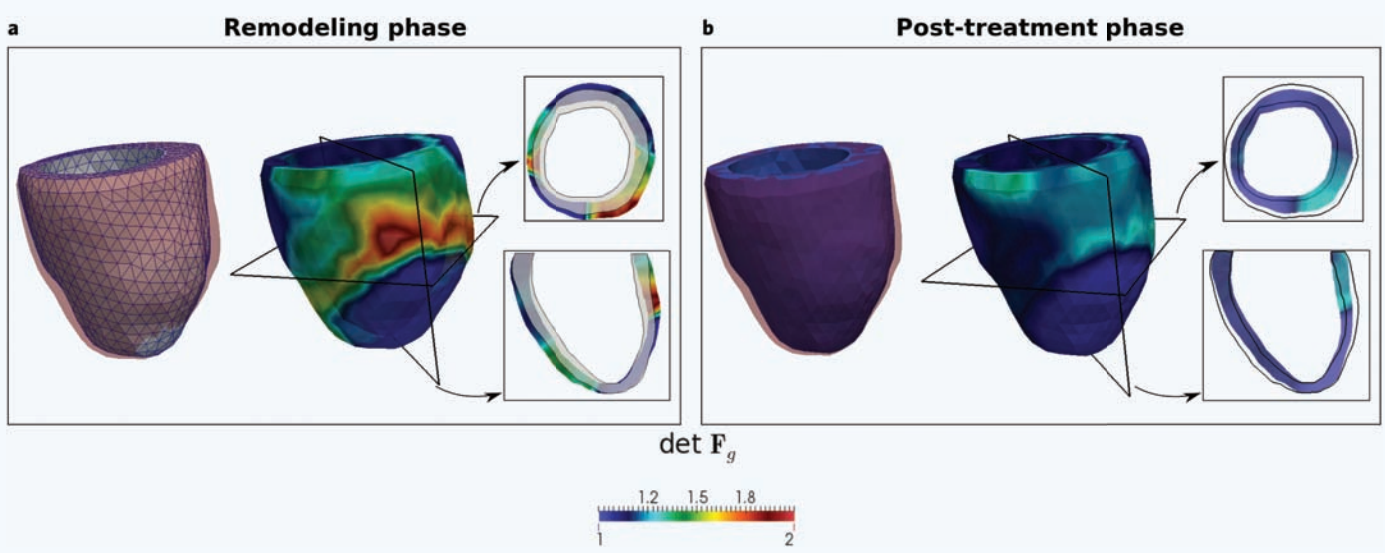

Figure 4 Geometrical changes of the LV during the (**a**) remodeling and (**b**) post-treatment phases. Leftmost: LV end-diastolic configuration at (a) cycle 5 (red) superimposed to that at cycle 1 (grey) and (b) cycle 15 (blue) superimposed to that in cycle 6 (red). Middle: Determinant of growth tensor det $\boldsymbol{F}_g$ at (a) cycle 5 and (b) cycle 15. Rightmost: corresponding long- and short-axis view. Black lines denote the same cross-section at the beginning of the two simulation phases. Note: det $\boldsymbol{F}_g$ is prescribed to remain constant at 1 in the infarct.

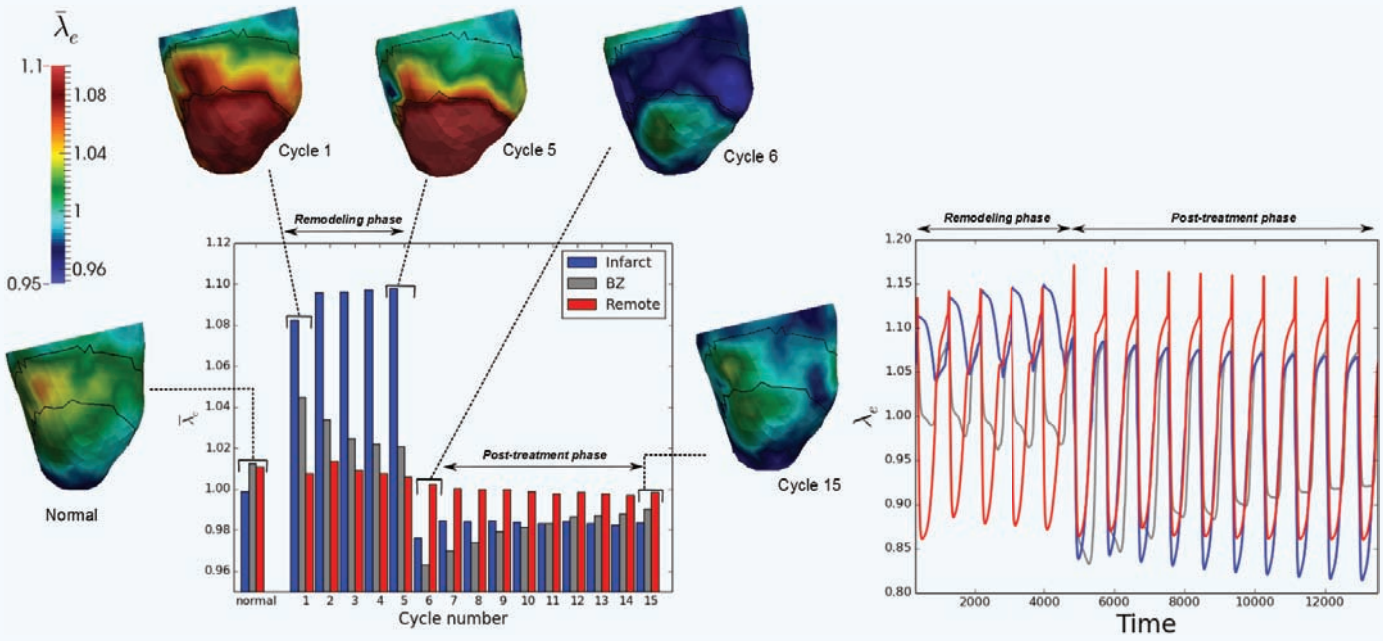

Figure 5 Left: time-averaged myofiber stretch $\bar{\lambda}_e$ in the infarct, borderzone and remote regions in the two simulation phases. Right: myofiber stretch taken from arbitary locations in these regions (same color scheme applied here). Note that the infarct and borderzone were regenerated at the end of cycle 5.

elastic myofiber stretch $\bar{\lambda}_e$ decreased and approached the values found in the normal LV. At the infarct, which was prescribed not to grow, the time-averaged elastic myofiber stretch did not decrease but increased slightly during the remodeling phase. We note that the reason why $\bar{\lambda}_e$ was highest at the infarct is because the infarct did not contract but underwent stretching even during the systole phase in a cardiac cycle.

Contractility was restored in both the infarct and borderzone in the post-treatment phase. The immediate effect of this alteration (in cycle 6) was a reduction in the values of $\bar{\lambda}_e$ in these two regions. The reduced values were below the corresponding homeostatic values found in the normal LV. In subsequent cycles of the post-treatment phase, the time-averaged elastic myofiber stretch in the borderzone and infarct increased and approached their respective homeostatic values.

DISCUSSION

Although computational models have been used to simulate the long-term effects of heart diseases and therapies[25,42,43], most models are only capable of simulating growth based on standard time points in the cardiac cycle (e.g. end-of-diastole or end-of-systole). As such, time-averaged, minima and maxima of local deformation signals cannot be applied as growth stimulant in these models, unless (of course), if these quantities are known a priori to correspond to particular time points in the cardiac cycle. Specific to volume overload where the cardiomyocytes elongates in its axial direction, an *in vivo* study on a rat model[37] suggests that the likely candidates for the hypertrophic stimuli are features of the time-varying volume signal, which are related to the myofiber stretch or strain. These features include the maximum, mean, amplitude, rates of rise and fall of the volume during the cardiac cycle. Additionally, *in-vitro* studies have also demonstrated that the hypertrophic gene expression is regulated by cyclic stretch of the cardiomyocytes[44,45]. Motivated by these studies, we have used the time-averaged myofiber stretch as the growth stimulant in our simulation. We have also, for the first time, applied the electromechanics-growth model to simulate the long-term effects of cardiac regenerative therapies. Our simulation results show features that are generally consistent with experimental and clinical studies, both in the remodeling and post-treatment phases.

Remodeling phase

During the remodeling phase, our model predicts a higher time-averaged myofiber stretch in both the borderzone and the infarct than that found in the normal LV (**Fig. 5**). As a result, growth occurs primarily in the borderzone. Globally, this local growth causes the LV to become dilated and more spherical (**Fig. 4**), which manifested as a shifting of the PV loop toward the right (**Fig. 3**).

All these features are consistent with experimental and clinical studies at the cellular and organ levels. First, abnormal stretch in the form of a reduced contractile deformation during systole is a widely observed feature found in the borderzone after MI[46,47]. Correspondingly, cardiomyocytes in the borderzone region would, when averaged over a cardiac cycle, undergo higher stretching. Second, cardiomyocytes in the borderzone of animal MI models displayed appreciable hypertrophy when compared to those in remote region[39,48]. For example, in the sheep heart, the cardiomyocytes' cross-sectional area was found to be about 70% higher than that in the remote region 2 weeks after MI[39]. The same observations were found in humans when isolated cardiomyocytes from explanted human hearts with ischemic-dilated cardiomyopathy were measured to be about 40% longer than those found in the normal heart[34]. Third, progressive LV dilation in the form of a parallel increase in both end-diastolic and end-systolic volumes is a pathophysiological feature of MI that is found in both humans and animals[49,50].

Post-treatment phase

Restoration of the infarct and borderzone contractilities to their normal values in our simulation led to an immediate increase in both stroke volume and EF. The time-averaged myofiber stretch also decreased immediately and fell below its corresponding homeostatic values in the infarct and borderzone upon restoration of their contractilities (**Fig. 5**). As a result, cardiomyocytes in the borderzone was predicted in our simulation to undergo atrophy

which led to a reversal of growth during this post-treatment phase (**Fig. 4**). This reversal was manifested globally by a decrease in the LV size that was reflected by a continuous shift of the PV loop toward the left (**Fig. 3**).

Cardiac regenerative therapies have, in recent years, garnered considerable interests. From the initial pilot studies on animal models where the results are mainly positive[9,51,52], these therapies have progressed into clinical trials. The review by Pfister *et al.*[53] summarizes the findings from the major recent clinical trials that investigate the use of different types of stem cells, such as bone marrow, mesenchymal and resident cardiac stem cells. The results from these clinical trials are mixed and controversial, with some showing insignificant clinical efficiacy[54–56], while others showing significant functional improvments and reverse remodeling post-treatment[57–60]. Clinical trials that found positive effects, including the POSEIDON study (mesenchymal stem cells)[58] and the SCIPO study (cardiac resident stem cells)[57], have shown that the infarct size reduces significantly (POSEIDON: 33%, SCIPO: 24–30%) at 4–12 months post-treatment. The significant reduction in the infarct size in the SCIPO study was accompanied by an statistically significant increase in EF by 8 pp., whereas the POSEIDON study found a 2 pp. increase in EF that is not statistically significant. These favorable effects were also found in another preclinical trial on the injection of mesenchymal and mononuclear stem cells[60]. In that study, a 20% decrease in infarct size, end-diastolic and end-systolic volumes, as well as a 4.5 pp. increase in EF were found after treatment. Our model, which of course is an idealization of these actual stem cell therapies, is able to replicate some of these findings, which include an increase in EF as well as decreases in end-diastolic and end-systolic volumes.

Besides these global functional and geometrical changes, postmortem analysis in porcine hearts implanted with mesenchymal stem cell have also found that the cardiomyocytes in the sub-endocardial rim of the MI are not hypertrophied when compared to those taken from the remote region[61]. It is unclear, however, as to whether these unhypertrophied cardiomyocytes are proliferated endogeneous cardiomyocytes or newly differentiated ones. Similar findings were also reported in rats treated with cardiosphere-derived cells[59], where the cross-sectional area of cardiomyocytes in the infarcted border zone was 20% smaller when compared to those found in the untreated rats. These results supported our model prediction that hypertrophy will regress in the borderzone's cardiomyocytes upon restoration of the LV contractility.

There are a number of factors that could affect the outcome of cardiac regenerative therapies and so, could possibly explain the large disparity in outcome found in these studies. These factors include the timing and methods of delivery, the optimal dosage and the recipient environment[62]. Little is known also about the myofiber architecture and the intrinsic contractility of the regenerated tissue. Given that the ventricular wall mechanics is sensitive to the myofiber architecture[63], the structural arrangement of the regenerated cardiomyocytes would have an impact on the treatment outcome. The current model can be extended to investigate and optimize these treatment parameters.

CONCLUSION

In summary, we have demonstrated that the electromechanics-growth model can reproduce features found in clinical observations and animal experiments of MI and infarct regeneration. The ability of our model in reproducing the findings from these studies also suggest, as with other *in-vivo* and *in-vitro* remodeling studies[37,44,45], that the time-averaged myofiber stretch is a probable stimuli for cardiomyocyte hypertrophy. This finding is significant in a way because the local prescription of growth constitutive law (at the gauss points) can reproduce large-scale remodeling of the ventricular geometry (such as the LV cavity volume) that is qualitatively consistent with the physical observations. Of course, whether the time-averaged myofiber stretch is the "true" hypertrophic stimuli can only be determined by testing the model with other pathologies (and treatments). In this aspect, the electromechanics-growth model is well set up for simulating heart diseases that involve long-term remodeling due to abnormalities in the excitation-contraction coupling mechanism and the associated treatments, e.g. cardiac resynchronization therapy for treatment of mechanical dyssynchrony due to left branch bundle block. We are currently pursuing research in this area.

Limitations

There are a number of limitations associated with this model. First, we did not consider the effects of infarct expansion which can cause a thinning of the infarct[64]. This event can occurs early in the time course of MI remodeling.

Second, we did not take into account that the borderzone can extend itself during remodeling[48]. Although the borderzone in our simulation expands in size via cellular hypertrophy, this effect is different from the extension of borderzone width when the adjacent healthy myocardium is progressively recruited into this dysfunctional zone.

Third, we did not take into account the immediate increase in LV wall volume after injection of new cells or retroviral particles that some of these cardiac therapies are based on. Although the injected volume is small compared to the LV wall volume in some studies (e.g., 2.5 mL injection *vs*. LV wall volume of ~150 mL[60]), there are other studies in which the injected volume is significant (e.g. 15 mL injection *vs*. LV wall volume of ~50 mL[61]). As shown in a number of modeling studies, the injection of new non-contractile materials into the LV wall can have an immediate impact on the regional mechanics that may affect the remodeling process[18,65].

Last, the timescale associated with each growth cycle would need to be properly characterized based on longitudinal data acquired from animal models and patients. In this aspect, it is important to recognize the fact that the growth timescale will differ across species, which have different metabolism rates. For example, the growth timescale in a rat infarct model is likely to be less than that in a swine infarct model as suggested in the experiments, where cardiomyocytes at the infarct borderzone were found to be hypertrophied by 30% in 3 days in a rat model[66] and by 70% in 6 weeks in a swine model[67]. To account for interspecies difference in the growth timescale, it may be useful to characterize the timescale based on physiological time (as opposed to chronological time) using empirical allometric scaling relationships[68]. Moreover, experiments have also suggested a different time scale for myocyte atrophy (reverse remodeling) from myocyte hypertrophy (remodeling)[35,69].

ACKNOWLEDGEMENTS

This work was supported by the Marie Curie International Outgoing Fellowship within the 7th European Community Framework Program (M.G.).

REFERENCES

1. Heidenreich, P.A. *et al*. Forecasting the future of cardiovascular disease in the United States: A policy statement from the American Heart Association. *Circulation* **123**, 933–944 (2011).
2. Szabo, T., Doehner, W. & Anker, S.D. Systolic heart failure. *N. Engl. J. Med*. **362**(16), 1545 (2010).
3. Antman, E.M. ACC/AHA Guidelines for the Management of Patients With ST- Elevation Myocardial Infarction–Executive Summary: A Report of the American College of Cardiology/American Heart Association Task Force on Practice Guidelines (Writing Committee to Revise the 1999. *Circulation* **110**(5), 588–636 (2004).
4. Velagaleti, R.S. *et al*. Long-term trends in the incidence of heart failure after myocardial infarction. *Circulation* **118**(20), 2057–2062 (2008).
5. Athanasuleas, C.L. *et al*. Surgical ventricular restoration in the treatment of congestive heart failure due to post-infarction ventricular dilation. *J. Am. Coll. Cardiol*. **44**(7), 1439–1445 (2004).
6. Nikolic, S.D. *et al*. Percutaneous implantation of an intraventricular device for the treatment of heart failure: Experimental results and proof of concept. *J. Card. Fail*. **15**, 790–797 (2009).
7. Garbern, J.C. & Lee, R.T. Cardiac stem cell therapy and the promise of heart regeneration. *Cell Stem Cell* **12**(6), 689–698 (2013).
8. Xin, M., Olson, E.N. & Bassel-Duby, R. Mending broken hearts: Cardiac development as a basis for adult heart regeneration and repair. *Nat. Rev. Mol. Cell Biol*. **14**(8), 529–541 (2013).

9. Qian, L. *In vivo* reprogramming of murine cardiac fibroblasts into induced cardiomyocytes. *Nature* **485**(7400), 593–598 (2012).
10. Williams, A.R. Intramyocardial stem cell injection in patients with ischemic cardiomyopathy: Functional recovery and reverse remodeling. *Circ. Res.* **108**(7), 792–796 (2011).
11. Marban, E. & Malliaras, K. Mixed results for bone marrow-derived cell therapy for ischemic heart disease. *JAMA* **308**(22), 2405–2406 (2012).
12. Constantino, J., Hu, Y. & Trayanova, N.A. A computational approach to understanding the cardiac electromechanical activation sequence in the normal and failing heart, with translation to the clinical practice of CRT. *Progr. Biophys. Mol. Biol.* **110**, 372–379 (2012).
13. Fomovsky, G.M., MacAdangdang, J.R., Ailawadi, G. & Holmes, J.W. Model-based design of mechanical therapies for myocardial infarction. *J. Cardiovasc. Transl. Res.* **4**, 82–91 (2011).
14. Kerckhoffs, R.C.P. *et al*. Ventricular dilation and electrical dyssynchrony synergistically increase regional mechanical nonuniformity but not mechanical dyssynchrony: A computational model. *Circulation* **3**(4), 528–536 (2010).
15. Lee, L.C. *et al*. Patient-specific finite element modeling of the Cardiokinetix Parachute device: Effects on left ventricular wall stress and function. *Med. Biol. Eng. Comput.* **52**, 557–566 (2014).
16. Lee, L.C. *et al*. Algisyl-LVR™ with coronary artery bypass grafting reduces left ventricular wall stress and improves function in the failing human heart. *Int. J. Cardiol.* **168**(3), 2022–2028 (2013).
17. Lee, L.C. *et al*. Analysis of patient-specific surgical ventricular restoration importance of an ellipsoidal left ventricular geometry for diastolic and systolic function. *J. Appl. Physiol.* (115), 136–144 (2013).
18. Wall, S.T. *et al*. Theoretical impact of the injection of material into the myocardium: A finite element model simulation. *Circulation* **114**, 2627–2635 (2006).
19. Wenk, J.F. *et al*. A method for automatically optimizing medical devices for treating heart failure: Designing polymeric injection patterns. *J. Biomech. Eng.* **131**(12), 121011 (2009).
20. Genet, M. *et al*. Modeling pathologies of diastolic and systolic heart failure. *Ann. Biomed. Eng.* **44**(1), 112–127 (2016).
21. Göktepe, S., Abilez, O.J., Parker, K.K. & Kuhl, E. A multiscale model for eccentric and concentric cardiac growth through sarcomerogenesis. *J. Theor. Biol.* **265**(3), 433–442 (2010).
22. Kerckhoffs, R.C.P., Omens, J.H. & McCulloch, A.D. A single strain-based growth law predicts concentric and eccentric cardiac growth during pressure and volume overload. *Mech. Res. Commun.* **42**, 40–50 (2012).
23. Lee, L.C. *et al*. A computational model that predicts reverse growth in response to mechanical unloading. *Biomech. Model. Mechanobiol.* **14**, 217–29 (2015).
24. Kerckhoffs, R.C.P., Omens, J.H. & McCulloch, A.D. Mechanical discoordination increases continuously after the onset of left bundle branch block despite constant electrical dyssynchrony in a computational model of cardiac electromechanics and growth. *Europace* **14**, v65–v72 (2012).
25. Klepach, D. *et al*. Growth and remodeling of the left ventricle: A case study of myocardial infarction and surgical ventricular restoration. *Mech. Res. Commun.* **42**, 134–141 (2012).
26. Lee, L.C., Sundnes, J., Genet, M., Wenk, J.F. & Wall, S.T. An integrated electromechanical-growth heart model for simulating cardiac therapies. *Biomech. Model. Mechanobiol.* doi: 10.1007/s10237-015-0723-8 (in press).
27. Burkhoff, D., Klotz, S. & Mancini, D.M. LVAD-induced reverse remodeling: Basic and clinical implications for myocardial recovery. *J. Card. Fail.* **12**(3), 227–239 (2006).
28. Sundnes, J., Wall, S.T., Osnes, H., Thorvaldsen, T. & McCulloch, A.D. Improved discretisation and linearisation of active tension in strongly coupled cardiac electro-mechanics simulations. *Comput. Methods Biomech. Biomed. Eng.* **17**(6), 604–615 (2014).
29. Winslow, R.L., Rice, J., Jafri, S., Marban, E. & O'Rourke, B. Mechanisms of altered excitation-contraction coupling in canine tachycardia-induced heart failure, II: Model studies. *Circ. Res.* **84**(5), 571–586 (1999).
30. Rice, J.J. *et al*. Approximate model of cooperative activation and crossbridge cycling in cardiac muscle using ordinary differential equations. *Biophys. J.* **95**(5), 2368–2390 (2008).
31. Guccione, J.M. *et al*. Passive material properties of intact ventricular myocardium determined from a cylindrical model. *J. Biomech. Eng.* **113**(1), 42–55 (1991).
32. Holzapfel, G. *Nonlinear Solid Mechanics: A Continuum Approach for Engineering*. John Wiley, p. 34 (2000).
33. Rodriguez, E.K. *et al*. Stress-dependent finite growth in soft elastic tissues. *J. Biomech.* **27**(4), 455–467 (1994).
34. Gerdes, A.M. Structural remodeling of cardiac myocytes in patients with ischemic cardiomyopathy. *Circulation* **86**(2), 426–430 (1992).
35. Gerdes, A.M. Regression of cardiac hypertrophy after closing an aortocaval fistula in rats. *Am. J. Physiol.* **268**(6 Pt. 2), H2345–H2351 (1995).
36. Hutchinson, K.R. *at al*. Temporal pattern of left ventricular structural and functional remodeling following reversal of volume overload heart failure. *J. Appl. Physiol.* **111**(6), 1778–1788 (2011).
37. Holmes, J.W. Candidate mechanical stimuli for hypertrophy during volume overload. *J. Appl. Physiol.* **97**, 1453–1460 (2004).
38. Genet, M. *et al*. A novel method for quantifying smooth regional variations in myocardial contractility within an infarcted human left ventricle based on delay-enhanced magnetic resonance imaging. *J. Biomech. Eng.* **137**(8), 081009 (2015).
39. Shimkunas, R. *et al*. Myofilament dysfunction contributes to impaired myocardial contraction in the infarct border zone. *AJP Hear. Circ. Physiol.* **307**, H1150–H1158 (2014).
40. Streeter, D.D. *et al*. Fiber orientation in the canine left ventricle during diastole and systole. *Circ. Res.* **24**(3), 339–347 (1969).
41. Niederer, S.A. *et al*. Verification of cardiac tissue electrophysiology simulators using an N-version benchmark. *Philos. Trans. R. Soc. A Math. Phys. Eng. Sci.* **369**(1954), 4331–4351 (2011).
42. Göktepe, S. *et al*. A multiscale model for eccentric and concentric cardiac growth through sarcomerogenesis. *J. Theor. Biol.* **265**(3), 433–442 (2010).
43. Rausch, M.K. *et al*. Computational modeling of growth: Systemic and pulmonary hypertension in the heart. *Biomech. Model. Mechanobiol.* **10**, 799–811 (2011).
44. Haggart, C.R. *et al*. Effects of stretch and shortening on gene expression in intact myocardium. *Physiol. Genomics* **46**(2), 57–65 (2014).
45. Torsoni, A.S. *et al*. Focal adhesion kinase is activated and mediates the early hypertrophic response to stretch in cardiac myocytes. *Circ. Res.* **93**(2), 140–147 (2003).
46. Ashikaga, H. *et al*. Electromechanical analysis of infarct border zone in chronic myocardial infarction. *Am. J. Physiol. Heart Circ. Physiol.* **289**, H1099–H1105 (2005).
47. Kramer, C.M. *et al*. Regional differences in function within noninfarcted myocardium during left ventricular remodeling. *Circulation* **88**, 1279–1288 (1993).
48. Jackson, B.M. *et al*. Extension of borderzone myocardium in postinfarction dilated cardiomyopathy. *J. Am. Coll. Cardiol.* **40**(6), 1160–1167 (2002).
49. McCall, F.C. *et al*. Myocardial infarction and intramyocardial injection models in swine. *Nat. Protoc.* **7**(8), 1479–1496 (2012).
50. Sutton, M.G.S.J. & Sharpe, N. New frontiers left ventricular remodeling after myocardial infarction pathophysiology and therapy. *Circulation* **101**, 2981–2988 (2000).
51. Dawn, B. *et al*. Cardiac stem cells delivered intravascularly traverse the vessel barrier, regenerate infarcted myocardium, and improve cardiac function. *Proc. Natl. Acad. Sci. U. S. A.* **102**(10), 3766–3771 (2005).
52. Li, X. *et al*. Intramyocardial injection of pig pluripotent stem cells improves left ventricular function and perfusion: A study in a porcine model of acute myocardial infarction. *PLoS One* **8**(6), e66688 (2013).
53. Pfister, O. *et al*. Regenerative therapy for cardiovascular disease. *Transl. Res.* **163**(4), 307–320 (2014).
54. Lunde, K. *et al*. Intracoronary injection of mononuclear bone marrow cells in acute myocardial infarction. *N. Engl. J. Med.* **355**(12), 1199–1209 (2006).
55. Meyer, G.P. *et al*. Intracoronary bone marrow cell transfer after myocardial infarction: Eighteen months' follow-up data from the randomized, controlled BOOST (Bone marrow transfer to enhance ST-elevation infarct regeneration) trial. *Circulation* **113**(10), 1287–1294 (2006).
56. Roncalli, J. *et al*. Intracoronary autologous mononucleated bone marrow cell infusion for acute myocardial infarction: Results of the randomized multicenter BONAMI trial. *Eur. Heart J.* **32**(14), 1748–1757 (2011).
57. Bolli, R. *et al*. Cardiac stem cells in patients with ischaemic cardiomyopathy (SCIPIO): Initial results of a randomised phase 1 trial. *Lancet* **378**(9806), 1847–1857 (2011).
58. Hare, J.M. *et al*. Comparison of allogeneic *vs.* autologous bone marrow-derived mesenchymal stem cells delivered by transendocardial injection in patients with ischemic cardiomyopathy. *JAMA* **308**(22), 2369 (2012).
59. Makkar, R.R. *et al*. Intracoronary cardiosphere-derived cells for heart regeneration after myocardial infarction (CADUCEUS): A prospective, randomised phase 1 trial. *Lancet* **379**(9819), 895–904 (2012).
60. Williams, A.R. *et al*. Intramyocardial stem cell injection in patients with ischemic cardiomyopathy: Functional recovery and reverse remodeling. *Circ. Res.* **108**(7), 792–796 (2011).
61. Amado, L.C. *et al*. Multimodality noninvasive imaging demonstrates *in vivo* cardiac regeneration after mesenchymal stem cell therapy. *J. Am. Coll. Cardiol.* **48**(10), 2116–2124 (2006).
62. Karantalis, V. *et al*. Cell-based therapy for prevention and reversal of myocardial remodeling. *Am. J. Physiol. Heart Circ. Physiol.* **303**(3), H256–H270 (2012).
63. Geerts, L. *et al*. Towards patient specific models of cardiac mechanics: A sensitivity study. *Lect. Notes Comput. Sci.* **2674**, 81–90 (2003).
64. Weisman, H.F. & Healy, B. Myocardial infarct expansion, infarct extension, and reinfarction: Pathophysiologic concepts. *Prog. Cardiovasc. Dis.* **30**(2), 73–110 (1987).
65. Lee, L.C. *et al*. Bioinjection treatment: Effects of post-injection residual stress on left ventricular wall stress. *J. Biomech.* **47**(12), 3115–3119 (2014).
66. Anversa, P., Ricci, R. & Olivetti, G. Quantitative structural analysis of the myocardium during physiologic growth and induced cardiac hypertrophy: A review. *J. Am. Coll. Cardiol.* **7**(5), 1140–1149 (1986).
67. Angeli, F.S. *et al*. Left ventricular remodeling after myocardial infarction: Characterization of a swine model on beta-blocker therapy. *Comp. Med.* **59**(3), 272–279 (2009).
68. Schmid-Nielson, K. *Scaling: Why Is Animal Size So Important*? (Cambridge University Press, 1984).
69. Hutchinson, K.R., Stewart, J.A. & Lucchesi, P.A. Extracellular matrix remodeling during the progression of volume overload-induced heart failure. *J. Mol. Cell. Cardiol.* **48**(3), 564–569 (2010).